Adsorption of Polymeric Micelles and Vesicles on a Surface Investigated by Quartz Crystal Microbalance

ARTICLE *in* THE JOURNAL OF PHYSICAL CHEMISTRY B · NOVEMBER 2006

Impact Factor: 3.3 · DOI: 10.1021/jp064273d · Source: PubMed

5 AUTHORS, INCLUDING:

Xuechang Zhou
Shenzhen University
29 PUBLICATIONS **444** CITATIONS
SEE PROFILE

Jing ji
Fudan University
7 PUBLICATIONS **131** CITATIONS
SEE PROFILE

Lifeng Yan
University of Science and Technology of China
120 PUBLICATIONS **3,026** CITATIONS
SEE PROFILE

Guangzhao Zhang
University of Science and Technology of China
203 PUBLICATIONS **4,079** CITATIONS
SEE PROFILE

Adsorption of Polymeric Micelles and Vesicles on a Surface Investigated by Quartz Crystal Microbalance

Yunfeng Yan, Xuechang Zhou, Jing Ji, Lifeng Yan, and Guangzhao Zhang*

Hefei National Laboratory for Physical Sciences at Microscale, Department of Chemical Physics, University of Science and Technology of China, Hefei, Anhui, China

Received: July 7, 2006; In Final Form: August 20, 2006

Polystyrene-*b*-poly(*N*-isopropylacrylamide) (PS-*b*-PNIPAM) diblock copolymers either with or without thiol end groups, depending on the relative length of the two blocks, form micelles or vesicles in water. The adsorption of such micelles or vesicles on a gold surface from aqueous solution was investigated in situ at 20 °C by use of a quartz crystal microbalance with dissipation monitoring (QCM-D). The changes in frequency (Δf) and dissipation (ΔD) revealed that the micelles and vesicles without thiol groups were intact with some deformation when they were deposited on the surface. On the other hand, the micelles and vesicles with thiol groups at the end of PNIPAM blocks would transform into trilayers due to the strong interaction between thiols and gold surface.

Introduction

The adsorption of micelles or vesicles on a solid surface creates supported layers or membranes. The formation of such layers as model systems is important for our understanding the behavior of membrane-bound proteins, cell−cell interaction processes, and biological signal transduction.[1−3] The adsorption of polymeric micelles from solution has been extensively investigated both theoretically[4−7] and experimentally.[8−21] It has been predicted that the micelles are not directly adsorbed but serve as the reservoir of the free chains if the soluble block is repelled strongly by the surface.[4] However, when the interaction between the nonsoluble block and the surface overcomes the repulsion, the micelles transform into a layer composed of a dense inner layer and an extended outer layer. If the soluble block is preferentially adsorbed, the micelle forms a sandwich structure with two swollen layers and one dense layer in between.[8] Actually, the structural transformation of micelles depends on not only the adsorption but also the disruption, fusion, and rearrangement during the adsorption. Structural transformation of vesicles is even more complex. Theoretical[22,23] and experimental[24−33] studies have shown that the transformation of lipid vesicles is governed by the balance between the overall bending and adhesion energies.

The kinetics of the adsorption can give information about the structural transformation of micelles and vesicles. Previous studies revealed a three-stage adsorption of micelles, that is, an incubation period, a fast growth of the adsorbed layer, and a slow adsorption, where structural transformation of the micelles occurred.[19−21] Since the kinetics studies are still limited, the mechanism of the structural transformation of either micelles or vesicles on a surface is largely unknown.

We have prepared polystyrene-*b*-poly(*N*-isopropylacrylamide) (PS-*b*-PNIPAM) diblock copolymers via reversible addition fragmentation chain transfer (RAFT) polymerization.[34] Such block copolymers can form micelles or vesicles in water, depending on the ratio of the length of the two blocks. Because the PNIPAM block can interact with the gold surface,[35] the micelles and vesicles can be physically adsorbed on the gold surface with their coronas. On the other hand, the dithiobenzoate group at the end of the PNIPAM block can be reduced into a thiol group by $NaBH_4$ in aqueous solution. Due to the strong coupling between the thiol group and gold,[36] the micelles or vesicles with a number of thiol groups on the periphery of their coronas can be strongly tethered on the gold surface. In the present study, we report the adsorption and structural transformation of such micelles and vesicles investigated by use of a quartz crystal microbalance.

Experimental Section

Materials. Details for synthesis of the diblock copolymers can be found elsewhere.[34] Molecular weights and molecular weight distributions (M_w/M_n) were determined by gel-permeation chromatography (GPC) on a Waters 150C by use of monodisperse polystyrene as the calibration standard and tetrahydrofuran (THF) as the eluent with a flow rate of 1.0 mL/min. For PS_{207}-*b*-$PNIPAM_{176}$ containing 207 styrene units and 176 NIPAM units, $M_w/M_n = 1.20$; for PS_{207}-*b*-$PNIPAM_{357}$ with a longer PNIPAM block, $M_w/M_n = 1.17$. Sodium borohydride ($NaBH_4$, China Medicine Group Co.) and other reagents were used as received.

Preparation of Micelles and Vesicles. PS_{207}-*b*-$PNIPAM_{357}$ micelles and PS_{207}-*b*-$PNIPAM_{176}$ vesicles were prepared by mixing the polymer solution in THF with Milli-Q water by use of a T-shaped syringe mixer with three channels and a Sp100i syringe pump, followed by dialysis at 20 °C.[34] The micelles and vesicles with thiol end groups at PNIPAM blocks were prepared by reduction of dithiobenzoate groups. Typically, 20 μL of 1.0 M $NaBH_4$ aqueous solution was added to 15 mL of polymer solution with a concentration of 1.0×10^{-4} g/mL. The solution stood at 4 °C for about 1 week so that the dithiobenzoate groups were completely reduced into thiol groups.[37] The solution was dialyzed against Milli-Q water by use of a semipermeable membrane with a cutoff molar mass of 3500 g/mol for 2 days to remove the metal ions.

Laser Light Scattering. A commercial LLS spectrometer (ALV/DLS/SLS-5022F) equipped with a multi-τ digital time

* To whom correspondence should be addressed.

10.1021/jp064273d CCC: $33.50
Published on Web 09/22/2006

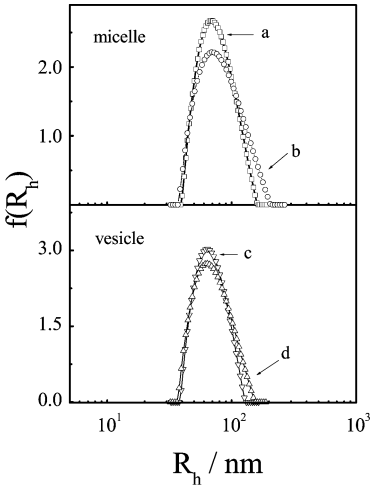

Figure 1. Hydrodynamic radius distributions $f(R_h)$ of the aggregates, where the polymer concentration was 1.0×10^{-4} g/mL: (a) PS_{207}-*b*-$PNIPAM_{357}$ micelles; (b) HS-PS_{207}-*b*-$PNIPAM_{357}$ micelles; (c) PS_{207}-*b*-$PNIPAM_{176}$ vesicles; (d) HS-PS_{207}-*b*-$PNIPAM_{176}$ vesicles.

correlation (ALV5000) and a cylindrical 22 mW Uniphase He−Ne laser ($\lambda_0 = 632$ nm) as the light source was used. The solutions were clarified by use of a 0.45 μm Millipore filter to remove dust before measurements. All the LLS measurements were performed at 20 °C. The root-mean-square radius of gyration $\langle R_g^2 \rangle_z^{1/2}$ (written as $\langle R_g \rangle$) was obtained from the angular dependence of the absolute excess time-average scattering intensity or the Rayleigh ratio $R_{vv}(q)$ in static LLS.[38,39] The intensity−intensity time correlation function $G^{(2)}(t,q)$ was measured to determine the line-width distribution $G(\Gamma)$ in dynamic LLS.[40] For diffusive relaxation, Γ is related to the translational diffusion coefficient (D) of the scattering object (polymer chain or colloid particle) in dilute solution or dispersion by $D = (\langle \Gamma \rangle / q^2)_{C \to 0, q \to 0}$ and further to hydrodynamic radius (R_h) from the Stokes−Einstein equation: $R_h = k_B T/(6\pi\eta D)$, where η, k_B, and T are the solvent viscosity, the Boltzmann constant, and the absolute temperature, respectively. Hydrodynamic radius distribution $f(R_h)$ was calculated from the Laplace inversion of a corresponding measured $G^{(2)}(t, q)$ by use of the CONTIN program. All the dynamic LLS measurements were conducted at a scattering angle (θ) of 15°.

High-Resolution Transmission Electron Microscopy. A JEOL2011 high-resolution transmission electron microscope was used to observe the morphologies of the micelles and vesicles at an acceleration voltage of 200 kV. A drop of a micelle or vesicle solution with a concentration of 1.0×10^{-4} g/mL was deposited onto a carbon-coated copper mesh grid. Then the sample was freeze-dried for the observation.

Quartz Crystal Microbalance Measurements. Quartz crystal microbalance with dissipation monitoring (QCM-D) and the AT-cut quartz crystal with a fundamental resonant frequency of 5 MHz and a diameter of 14 mm were from Q-sense AB.[41] The quartz crystal was mounted in a fluid cell with one side exposed to the solution. The constant (C) of the crystal used was 17.7 ng/cm^2 Hz. The frequency shift was measurable to within ±1 Hz in aqueous medium. The effects of surface roughness were minimized by using highly polished crystals with a root-mean-square roughness less than 3 nm.[42]

When a quartz crystal is excited to oscillate in the thickness shear mode at its fundamental resonant frequency (f_0) by applying a RF voltage across the electrodes near the resonant frequency, a small layer added to the electrodes induces a decrease in resonant frequency (Δf), which is proportional to

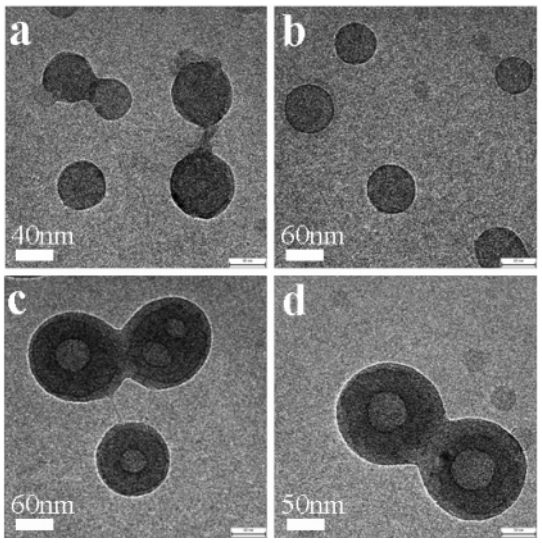

Figure 2. HRTEM images of the aggregates: (a) PS_{207}-*b*-$PNIPAM_{357}$ micelles; (b) HS-PS_{207}-*b*-$PNIPAM_{357}$ micelles; (c) PS_{207}-*b*-$PNIPAM_{176}$ vesicles; (d) HS-PS_{207}-*b*-$PNIPAM_{176}$ vesicles.

the mass (Δm) of the layer. In a vacuum or air, if the added layer is rigid, evenly distributed, and much thinner than the crystal, Δf is related to Δm and the overtone number ($n = 1, 3, 5, ...$) by the Sauerbrey equation:[43]

$$\Delta m = -\frac{\rho_q l_q}{f_0}\frac{\Delta f}{n} \quad (1)$$

where f_0 is the fundamental frequency and ρ_q and l_q are the specific density and thickness of the quartz crystal, respectively. The dissipation factor (ΔD) is defined by $\Delta D = E_d/2\pi E_s$, where E_d is the energy dissipated during one oscillation and E_s is the energy stored in the oscillating system. The measurement of ΔD is based on the fact that the voltage over the crystal decays exponentially as a damped sinusoidal when the driving power of a piezoelectric oscillator is switched off.[41] By switching the driving voltage on and off periodically, we can simultaneously obtain a series of the changes of the resonant frequency and the dissipation factor. The solvent effect on the frequency and dissipation responses can be removed by using the corresponding solvent as the reference.[44,45]

A measurement of the adsorption was initiated by switching the liquid exposed to the gold-coated quartz resonator from a pure solvent to a polymer solution with a concentration of 1.0×10^{-4} g/mL. Δf and ΔD values from the fundamental were usually noisy because of insufficient energy trapping and thus were discarded.[46] All experiments were conducted at 20 ± 0.02 °C.

Results and Discussion

Figure 1 shows typical hydrodynamic radius distributions $f(R_h)$ of the micelles and vesicles before and after reduction, where the concentrations were 1.0×10^{-4} g/mL. For PS_{207}-*b*-$PNIPAM_{357}$ micelles, $\langle R_h \rangle = 73$ nm. On the other hand, we were able to obtain $\langle R_g \rangle = 62$ nm from static LLS measurements. Accordingly, $\langle R_g \rangle / \langle R_h \rangle = 0.85$. Likewise, for HS-$PS_{207}$-*b*-$PNIPAM_{357}$ micelles, $\langle R_h \rangle = 72$ nm, $\langle R_g \rangle = 61$ nm, and $\langle R_g \rangle / \langle R_h \rangle = 0.85$. For PS_{207}-*b*-$PNIPAM_{176}$ vesicles, $\langle R_h \rangle = 65$ nm, $\langle R_g \rangle = 63$ nm, and $\langle R_g \rangle / \langle R_h \rangle = 0.97$. For HS-$PS_{207}$-*b*-$PNIPAM_{176}$ vesicles, $\langle R_h \rangle = 63$ nm, $\langle R_g \rangle = 60$ nm, and $\langle R_g \rangle / \langle R_h \rangle = 0.95$. Clearly, the reduction almost did not change the size of either the micelles or the vesicles. It is known that the ratio $\langle R_g \rangle / \langle R_h \rangle$

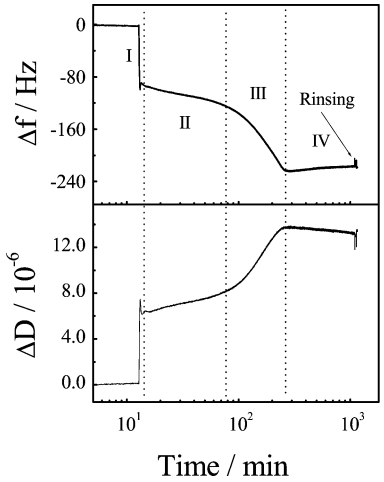

Figure 3. Changes in frequency (Δf) and dissipation (ΔD) of PS_{207}-*b*-$PNIPAM_{357}$ micelles as a function of logarithmic time.

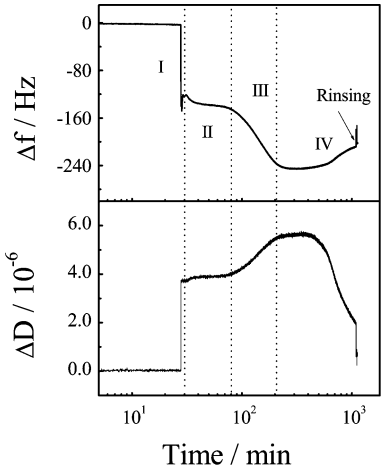

Figure 4. Changes in frequency (Δf) and dissipation (ΔD) of HS-PS_{207}-*b*-$PNIPAM_{357}$ micelles as a function of logarithmic time.

can reflect the conformation of a polymer or the structure of aggregates. For uniform nondraining sphere, hyperbranched cluster, and random coil structures, $\langle R_g\rangle/\langle R_h\rangle$ is ~0.774, 1.0−1.2, and 1.5−1.8, respectively.[47] The fact that the reduction almost did not change $\langle R_g\rangle/\langle R_h\rangle$ for either the micelles or the vesicles indicates that their morphologies were not changed. HRTEM images of the micelles and vesicles before and after the reduction, shown in Figure 2, further revealed that the size and morphology of the micelles and the vesicles did not change after the reduction.

Figure 3 shows the changes in frequency (Δf) and dissipation (ΔD) of the quartz resonator immersed in PS_{207}-*b*-$PNIPAM_{357}$ micelle solution before reduction as a function of logarithmic time. It is known that the frequency is related to the hydrodynamic mass of the layer, whereas the dissipation is related to the thickness and looseness.[41] The slight changes in both Δf and ΔD after the rinsing indicate the saturation of the gold surface. Obviously, the adsorption exhibits four-regime kinetics. At the initial stage (regime I), Δf significantly decreases and ΔD markedly increases. Actually, such a phenomenon was also observed in the other micelles and vesicles in the present work. This is because the deposition of a monolayer of micelles or vesicles onto a bare surface occurs in only a few minutes, which appears instantaneous on a logarithmic scale. Since PS has a glass transition temperature above the measurement temperature, PS blocks are not expected to interact with the gold surface. Our previous study showed that the interaction between dithiobenzoate groups and gold surface in an aqueous solution was very weak.[48] However, PNIPAM chains proved segmentally adsorbed on a gold surface,[35] so that the micelles could interact with the gold surface with their PNIPAM coronas. Moreover, since PNIPAM blocks form stretched brushes,[34] only a small amount of their segments are expected to contact the surface. Accordingly, the adsorbed micelles should be separated spheres with a small deformation.

In regime II, the adsorption becomes much slower, reflected in a slight change of Δf and ΔD. This is because the adsorption was hindered by the micelles already adhered on the surface. The relatively sharp decrease in Δf and increase in ΔD in regime III demonstrate that the adsorption was accelerated; namely, more micelles were adsorbed. Penn and co-workers[49−52] found that the grafting of amine end-terminated polystyrene chains grafted on the surface of silicate glass in a good solvent also exhibited such an acceleration, which was attributed to the cooperative lateral contraction of incoming and grafted chains. The acceleration in the present case implies that the already adsorbed micelles have rearranged in regime II so that the incoming micelles could be further adsorbed.

In regime IV, the slight increase in Δf and decrease in ΔD suggest the adsorbed micelles underwent some deformation or fusion with some water molecules bound on the PNIPAM shell expelled. Since PNIPAM blocks are dense brushes[34] and the interaction between PNIPAM segments and the gold surface is relatively weak, such deformation or fusion is expected to be limited. Finally, the saturation attained equilibrium so that both Δf and ΔD became constants.

Figure 4 shows the changes in frequency (Δf) and dissipation (ΔD) of the quartz resonator immersed in PS_{207}-*b*-$PNIPAM_{357}$ micelle solution with thiol groups (HS-PS_{207}-*b*-$PNIPAM_{357}$) as a function of logarithmic time. The adsorption of HS-PS_{207}-*b*-$PNIPAM_{357}$ micelles also exhibits four-regime kinetics. Regimes I−III are similar to those for PS_{207}-*b*-$PNIPAM_{357}$ micelles; namely, the micelles were quickly adsorbed in regime I, rearranged in regime II, and further adsorbed in regime III. However, HS-PS_{207}-*b*-$PNIPAM_{357}$ micelles exhibit a relatively remarkable increase in Δf until it reaches a constant in regime IV, implying that some polymer chains or water molecules left the layer. Meanwhile, the marked decrease in ΔD demonstrates that the layer became denser. Figures 3 and 4 show that the maximum Δf values in regime III for the two micelles are close, but HS-PS_{207}-*b*-$PNIPAM_{357}$ micelles exhibit a much smaller ΔD than PS_{207}-*b*-$PNIPAM_{357}$ micelles there, further indicating that the former transit into a more compact structure.

It is known that PS_{207}-*b*-$PNIPAM_{357}$ micelles are physically adsorbed on the gold surface with PNIPAM blocks. The relatively weak interaction between PNIPAM segments and the gold surface allows the micelles to deform and rearrange themselves with the structure intact. However, for HS-PS_{207}-*b*-$PNIPAM_{357}$ micelles, PNIPAM blocks contacting the gold surface could not only be segmentally adsorbed but also be strongly tethered on the surface with their thiol end groups, leading more PNIPAM blocks to be adsorbed on the surface. The micelles are expected to be hemispherelike. As the population of the adsorbed micelles increases, the surface becomes crowded, and the micelles could fuse with each other. Finally, they form a continuous trilayer with one thin PNIPAM layer contacting the gold surface and one thick PNIPAM layer on the top; between is the PS layer. Most of the chains in the micelles are expected to pack in the trilayer, although a few of them might be randomly adsorbed on the surface of the layer.

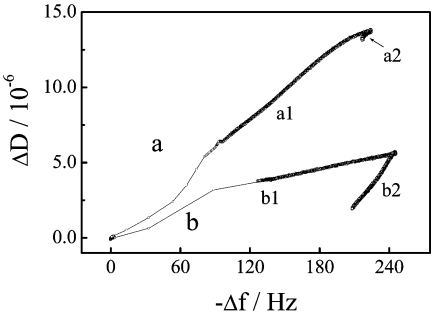

Figure 5. Plots of ΔD vs Δf for (a) PS_{207}-*b*-$PNIPAM_{357}$ micelles and (b) HS-PS_{207}-*b*-$PNIPAM_{357}$ micelles.

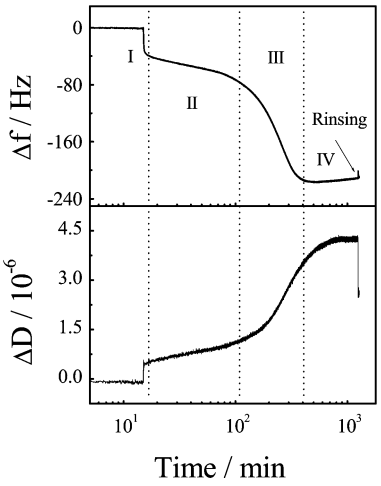

Figure 6. Changes in frequency (Δf) and dissipation (ΔD) of PS_{207}-*b*-$PNIPAM_{176}$ vesicles as a function of logarithmic time.

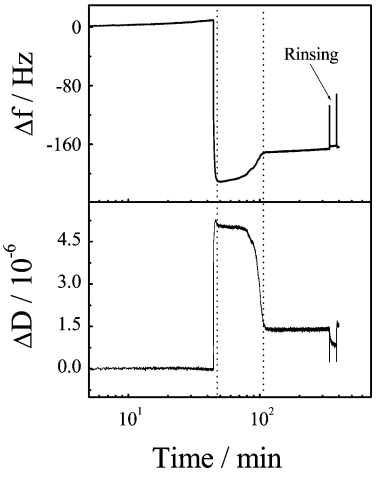

Figure 7. Changes in frequency (Δf) and dissipation (ΔD) of HS-PS_{207}-*b*-$PNIPAM_{176}$ vesicles as a function of logarithmic time.

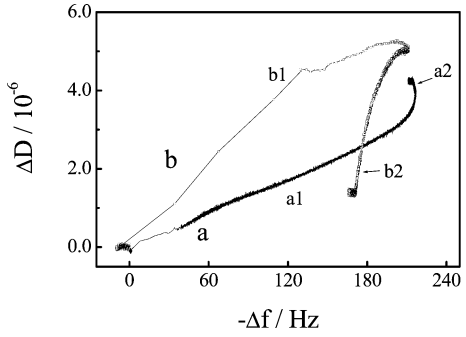

Figure 8. Plots of ΔD vs Δf for (a) PS_{207}-*b*-$PNIPAM_{176}$ vesicles and (b) HS-PS_{207}-*b*-$PNIPAM_{176}$ vesicles.

Due to the hydrophobic−hydrophilic balance, the unpacked chains would go back to the bulk solution, leading Δf to increase and ΔD to decrease in regime IV.

Figure 5 shows the ΔD versus Δf relationship. Such a relationship can give information about the deformation and transformation of the micelles.[53] The adsorption of each kind of micelles exhibits two kinetic processes. For PS_{207}-*b*-$PNIPAM_{357}$ micelles, regimes I−III in Figure 3 have the same ΔD versus Δf relationship (a1), implying that the micelles in these regimes have the same structure. Another slightly different kinetic process (a2) can be found in regime IV (Figure 3), suggesting some limited deformation or fusion of the micelles there. On the other hand, HS-PS_{207}-*b*-$PNIPAM_{357}$ micelles also show the same kinetic process (b1) in regimes I−III (Figure 4), suggesting that the structures of the adsorbed micelles in the regimes are almost the same. In regime IV (Figure 4), the micelles exhibit a quite different kinetic process (b2), suggesting a structural change of the micelles; namely, the micelles are fused and transformed into a trilayer.

Figure 6 shows the changes in frequency (Δf) and dissipation (ΔD) of the quartz resonator immersed in PS_{207}-*b*-$PNIPAM_{176}$ vesicle solution before reduction as a function of logarithmic time. Like the micelles, PS_{207}-*b*-$PNIPAM_{176}$ vesicles without thiol groups also exhibit four-regime kinetics of adsorption. In regime I, the significant decrease in Δf and increase in ΔD indicate that the vesicles were quickly adsorbed on the bare gold surface. As we discussed above, due to the weak segmental adsorption of PNIPAM blocks, the vesicles are expected to form deformed hollow spheres on the surface. In regime II, the slow decrease in Δf and increase in ΔD indicate that the adsorption was hindered by the micelles already adhered on the surface. In regime III, the marked decrease in Δf and increase in ΔD indicate that the incoming vesicles were further adsorbed after the rearrangement. As more vesicles are adsorbed on the surface, the vesicles would further deform and fuse. Like the case of PS_{207}-*b*-$PNIPAM_{357}$ micelles, such deformation and fusion should be limited. Δf and ΔD finally reach constants, indicating the saturation of the surface.

Figure 7 shows the changes in frequency (Δf) and dissipation (ΔD) of the quartz resonator immersed in HS-PS_{207}-*b*-$PNIPAM_{176}$ vesicle solution as a function of logarithmic time. In comparison with the micelles and vesicles discussed above, HS-PS_{207}-*b*-$PNIPAM_{176}$ vesicles show quite different adsorption kinetics. At the initial stage, Δf markedly decreases to a minimum value while ΔD increases to a maximum value, indicating the quick adsorption of the vesicles. Subsequently, Δf increases and ΔD decreases gradually until they reach constants. Such a phenomenon was previously observed by Keller et al.[23,24] for lipid vesicles on a SiO_2 surface, which was attributed to the transformation from vesicles to bilayers. In the present study, due to the strong hydrophobic association of PS blocks, the vesicles should be difficult to split. However, unlike the polymeric micelles, the hollow polymeric vesicles are unstable in curvature. As more and more PNIPAM blocks were tethered on the gold surface, the overall interaction between the gold surface and the thiol groups was strong enough to balance the overall bending energy of the vesicles. As a result, the vesicles split and transform into a trilayer. The water molecules trapped in the vesicles were expelled during the transformation, leading to the increase in Δf and decrease in ΔD. Note that, unlike the case in HS-PS_{207}-*b*-$PNIPAM_{357}$ micelles, both Δf and ΔD of HS-PS_{207}-*b*-$PNIPAM_{176}$ vesicles reached constants after the transformation, implying that almost all the chains in HS-PS_{207}-*b*-$PNIPAM_{176}$ vesicles pack in the

layer. This might be because the chains could reasonably pack on the surface with the rupture of the vesicles.

Figure 8 shows the ΔD versus Δf relationships of PS_{207}-*b*-$PNIPAM_{176}$ and HS-PS_{207}-*b*-$PNIPAM_{176}$ vesicles. Roughly, both of them exhibit two kinds of kinetic processes. For PS_{207}-*b*-$PNIPAM_{176}$ vesicles, the same kinetic process (a1) in regimes I−III (Figure 6) suggests that the vesicles on the surface still have the same structure after the adsorption and rearrangement, that is, the separated hollow spheres. The other kinetic process (a2) in regime IV suggests the deformation and fusion of the vesicles. The smooth turn between the two kinetics areas suggests a slight reorganization of the vesicles accompanying the adsorption. For HS-PS_{207}-*b*-$PNIPAM_{176}$ vesicles, the two kinetic processes (b1 and b2) of the adsorption further suggest that the vesicles underwent a vesicle-to-trilayer transition.

Conclusion

In conclusion, using quartz crystal microbalance with dissipation (QCM-D), we have investigated the adsorption and structural transformation of micelles and vesicles formed by PS-*b*-PNIPAM diblock copolymers on a gold surface in real time. Our results revealed that the interaction between the polymer chains and the gold surface plays a critical role in the structural deformation and transformation. Micelles and vesicles without thiol groups slightly underwent limited structural deformation and fusion when they were adsorbed on the surface. The micelles and vesicles with thiol groups were not only segmentally adsorbed but also tethered on the gold surface, leading to a large deformation and transformation.

Acknowledgment. The financial support of the National Natural Science Foundation (NNSF) of China (20474060) and The Chinese Academy of Sciences (KJCX2-SW-H14) is gratefully acknowledged.

References and Notes

(1) Watts, T. H.; Brian, A. A.; Kappler, J. W.; Marrack, P.; McConnell, H. M. *Proc. Natl. Acad. Sci. U.S.A.* **1984**, *81*, 7564.
(2) Nollert, P.; Kiefer, H.; Jähnig, F. *Biophys. J.* **1995**, *69*, 1447.
(3) Heyse, S. H.; Vogel, M.; Sänger, M.; Sigrist, H. *Protein Sci.* **1995**, *4*, 2532.
(4) Johner, A.; Joanny, J. F. *Macromolecules* **1990**, *26*, 5299.
(5) Marques, C. M.; Joanny, J. F.; Leibler, L. *Macromolecules* **1988**, *21*, 1051.
(6) van Lent, B.; Scheutjens, J. M. H. M. *Macromolecules* **1989**, *22*, 1931.
(7) Munch, M. R.; Gast, A. P. *Macromolecules* **1988**, *21*, 1366.
(8) Bijsterbosch, H. D.; Cohen Stuart, M. A.; Fleer, G. J. *Macromolecules* **1998**, *31*, 9281.
(9) Toomey, R.; Mays, J.; Yang, J.; Tirrell, M. *Macromolecules* **2006**, *39*, 2262.
(10) Parsonage, E.; Tirrell, M.; Watanabe, H.; Nuzzo, R. G. *Macromolecules* **1991**, *24*, 1987.
(11) Emoto, K.; Nagasaki, Y.; Kataoka, K. *Langmuir* **1999**, *15*, 5212.
(12) Huang, N. P.; Csucs, G.; Emoto, K.; Nagasaki, Y.; Kataoka, K.; Textor, M.; Spencer, N. D. *Langmuir* **2002**, *18*, 252.
(13) Tripp, C. P.; Hair, M. L. *Langmuir* **1996**, *12*, 3952.
(14) Brandani, P.; Stroeve, P. *Macromolecules* **2003**, *36*, 9492.
(15) Huguenard, C.; Varoqui, R.; Pefferkorn, E. *Macromolecules* **1991**, *24*, 2226.
(16) Tassin, J. F.; Siemens, R. L.; Tang, W. T.; Hadziioannou, G.; Swalen, J. D.; Smith, B. A. *J. Phys. Chem.* **1989**, *93*, 2106.
(17) Hahn, J.; Webber, S. E. *Langmuir* **2004**, *20*, 1489.
(18) Tiberg, F.; Malmsten, M.; Linse, P.; Lindman, B. *Langmuir* **1991**, *7*, 2723.
(19) Abraham, T.; Giasson, S.; Gohy, J. F.; Jerome, R.; Muller, B.; Stamm, M. *Macromolecules* **2000**, *33*, 6051.
(20) Munch, M. R.; Gast, A. P. *Macromolecules* **1990**, *23*, 2313.
(21) Halperin, A.; Tirrell, M.; Lodge, T. P. *Adv. Polym. Sci*. **1992**, *100*, 31.
(22) Lipowsky, R. *Phys. Rev. A* **1991**, *42*, 4768.
(23) Keller, C. A.; Kasemo, B. *J. Chem. Phys*. **2000**, *112*, 900.
(24) Keller, C. A.; Glasmastar, K.; Zhdanov, V. P.; Kasemo, B. *Phys. Rev. Lett.* **2000**, *84*, 5443.
(25) Keller, C. A.; Kasemo, B. *Biophys. J.* **1998**, *75*, 1397.
(26) Reimhult, E.; Höök, F.; Kasemo, B. *Langmuir* **2003**, *19*, 1681.
(27) Reviakine, I.; Brisson, A. *Langmuir* **2000**, *16*, 1806.
(28) Richter, R.; Mukhopadhyay, A.; Brisson, A. *Biophys. J.* **2003**, *85*, 3035.
(29) Richter, R. P.; Maury, N.; Brisson, A. R. *Langmuir* **2005**, *21*, 299.
(30) Cheng, Y.; Boden, N.; Bushby, R. J.; Clarkson, S.; Evans, S. D.; Knowles, P. F.; Marsh, A.; Miles, R. E. *Langmuir* **1998**, *14*, 839.
(31) Seantier, B.; Breffa, C.; Felix, O.; Decher, G. *Nano Lett*. **2004**, *4*, 5.
(32) Seantier, B.; Breffa, C.; Felix, O.; Decher, G. *J. Phys. Chem. B* **2005**, *109*, 21755.
(33) Xu, S.; Szymanski, G.; Lipkowski, J. *J. Am. Chem. Soc*. **2004**, *126*, 12276.
(34) Zhang, W.; Zhou, X.; Li, H.; Fang, Y.; Zhang, G. Z. *Macromolecules* **2005**, *38*, 909.
(35) Plunkett, M. A.; Wang, Z. H.; Rutland, M. W.; Johannsmann, D. *Langmuir* **2003**, *19*, 6837.
(36) Love, J. C.; Estroff, L. A.; Kriebel, J. K.; Nuzzo, R. G.; Whitesides, G. M. *Chem. Rev.* **2005**, *105*, 1103.
(37) Zhu, M. D.; Wang, L. Q.; Exarhos, G. J.; Li, A. D. Q. *J. Am. Chem. Soc.* **2004**, *126*, 2656.
(38) Zimm, B. H. *J. Chem. Phys*. **1948**, *16*, 1099.
(39) Chu, B. *Laser Light Scattering*, 2nd ed; Academic Press: New York, 1991.
(40) Berne, B.; Pecora, R. *Dynamic Light Scattering*, Plenum Press: New York, 1976.
(41) (a) Rodahl, M.; Höök, F.; Krozer, A.; Kasemo, B.; Breszinsky, P. *Rev. Sci. Instrum.* **1995**, *66*, 3924. (b) Voinova, M. V.; Rodahl, M.; Jonson, M.; Kasemo, B. *Phys. Scr*. **1999**, *59*, 391.
(42) Daikhin, L.; Urbakh, M. *Faraday Discuss.* **1997**, *107*, 27.
(43) Sauerbrey, G. *Z. Phys.* **1959**, *155*, 206.
(44) Kanazawa, K. Z.; Gordon, J. G., III. *Anal. Chem.* **1985**, *57*, 1770.
(45) (a) Stockbridge, C. D. In *Vacuum Microbalance Techniques*; Katz, M. J., Ed.; Plenum Press: New York, 1966. (b) Rodahl, M.; Kasemo, B. *Sens. Actuators, A* **1996**, *54*, 448.
(46) Bottom, V. E. *Introduction to Quartz Crystal Unit Design*; van Nostrand Reinhold Co.: New York, 1982.
(47) Burchard, W. In *Light Scattering Principles and Development*; Brown, W., Ed.; Clarendon Press: Oxford, U.K., 1996; p 439.
(48) Liu, G. M.; Yan, L. F.; Chen, X.; Zhang, G. Z. *Polymer* **2006**, *47*, 3157.
(49) Penn, L. S.; Hunter, T. F.; Lee, Y.; Quirk, R. P. *Macromolecules* **2000**, *33*, 1105.
(50) Penn, L. S.; Huang, H.; Sindkhedkar, M. D.; Rankin, S. E.; Chittenden, K.; Quirk, R. P.; Mathers, R. P.; Lee, Y. *Macromolecules* **2002**, *35*, 7054.
(51) Huang, H.; Penn, L. S.; Quirk, R. P.; Cheong, T. H. *Macromolecules* **2004**, *37*, 516.
(52) Huang, H.; Rankin, S. E.; Penn, L. S.; Quirk, R. P.; Cheong, T. H. *Langmuir* **2004**, *20*, 5770.
(53) Höök, F.; Rodahl, M.; Brezinski, P.; Kasemo, B.; Brezinski, P. *Proc. Natl. Acad. Sci. U.S.A.* **1998**, *95*, 12271.